Low-temperature thermochronology of the Indus Basin in central Ladakh, northwest India: Implications of Miocene–Pliocene cooling in the India-Asia collision zone

Gourab Bhattacharya[1*], Delores M. Robinson[1], Devon A. Orme[2], Yani Najman[3], Andrew Carter[4]

[1]Department of Geological Sciences and Center for Sedimentary Basin Studies, The University of Alabama, AL-35487, USA

[2]Department of Earth Sciences, Montana State University, MT-59717, USA

[3]Lancaster Environment Centre, Lancaster University, LA-14YQ, UK

[4]Department of Earth & Planetary Sciences, Birkbeck, University of London, WC1E 7HX, UK

**Corresponding author: gbhattacharya1@crimson.ua.edu*

Abstract: The India-Asia collision zone in Ladakh, northwest India, records a sequence of tectono-thermal events in the orogen interior following the intercontinental collision between India and Asia in early Cenozoic time. We present zircon fission-track, and zircon and apatite (U-Th)/He thermochronometric data from the Indus Basin sedimentary rocks located along the collision zone in central Ladakh, northwest India. From these data, we identify a post-depositional Miocene–Pliocene (~22–4 Ma) cooling phase within the India-Asia collision zone. Our ZFT cooling ages indicate that maximum basin temperatures exceeded 200 °C but stayed below 280–300 °C in the stratigraphically deeper marine and continental strata. Thermal modeling of zircon and apatite (U-Th)/He cooling ages suggest that post-depositional basin cooling initiated during the Early Miocene time by ~22–20 Ma, occurred throughout the basin across ZHe partial retention temperatures from ~20–10 Ma, and continued in the Pliocene time until at least ~4 Ma. We

attribute the burial of the Indus Basin to sedimentation and the overthrusting Great Counter thrust. The ensuing Miocene–Pliocene cooling resulted from erosion by the Indus River that transects the basin. A similar temporal cooling history is documented to the east in south Tibet along the India-Asia suture, and this study provides a regional framework upon which future works can explore the possible interrelationships between tectonic, geodynamic and geomorphological factors contributing to regional cooling along the strike of the India-Asia collision zone.

Keywords: Indus Basin, exhumation, cooling, thermochronology, India-Asia collision zone, Ladakh

1. Introduction

The India-Asia collision zone developed when the Neo-Tethyan ocean closed following continent-continent collision between India and Asia in early Cenozoic time (e.g., Searle, 2019; Kapp and DeCelles, 2019). The sedimentary basins along the collision zone present a natural laboratory to test models of deposition and exhumation in the interior of the Himalayan orogenic system. The collision zone in Ladakh, northwest (NW) India exposes the Indus Molasse or the Indus Basin sedimentary rocks (IBSR), which are a linear suite of deformed marine and continental strata that were discontinuously deposited from Late Cretaceous to Pliocene time (Figure 1; Garzanti and Van Haver, 1988; Searle et al., 1990; Clift et al., 2002; Henderson et al., 2010; 2011). Thus, the IBSR, which are exposed at the surface today, present an opportunity to study the pre- and syn-collisional tectono-thermal events associated with the evolution of the intercontinental suture zone between India and Asia. Knowing the timing and extent of suture zone basin exhumation is critical to understanding the surficial-to-lithospheric scale processes triggering it, which are intrinsically linked to the geological evolution of the orogenic hinterland.

Previous work on the IBSR thermal history along the India-Asia collision zone in NW India and coeval rocks along the collision zone in south Tibet yield different exhumation histories. Carrapa et al. (2014) present (U-Th)/He detrital zircon (ZHe) and apatite fission-track (AFT) cooling ages from the Late Oligocene–Early Miocene Kailas Formation of the Yarlung suture in south Tibet, which record basin exhumation from ~21–15 Ma. These cooling ages are interpreted to reflect incision by the paleo-Yarlung River as the Indian plate underthrusted beneath Asia. In addition, Tremblay et al. (2015) and Orme (2019) document Early–Middle Miocene (~21–11 Ma) cooling in the Gangdese batholith and the Xigaze forearc basin in south Tibet, thereby emphasizing that Miocene cooling along the India-Asia collision zone was a regional thermal event. By contrast,

in NW India, Tripathy-Lang et al. (2013) report ~52–28 Ma ZHe cooling ages from the Kailas-contemporaneous Late Oligocene Basgo Formation. Unlike post-depositional Miocene basin cooling as recorded in south Tibet, the ZHe cooling ages of the Basgo Formation in NW India are interpreted to be unreset after deposition and are attributed to exhumation of the source – the rapidly-eroding Indian margin (Tripathy-Lang et al., 2013). The only previously reported evidence of post-depositional Miocene heating and cooling in the IBSR is limited to two AFT ages of ~14–12 Ma (Clift et al., 2002) and a single AFT age of ~7 Ma (Schlup et al., 2003). However, ZFT, ZHe and AFT ages from the Ladakh batholith to the north of the IBSR indicate rapid cooling along the collision zone in NW India at ~26–18 Ma (Kirstein et al., 2006).

To determine if a Miocene cooling signal is present across different formations in the Indus Basin in NW India, we sampled the IBSR across 4 traverses in central Ladakh: Temesgam and Basgo sections in the west, Zanskar Gorge in the center, and Upshi-Lato section in the east (Figure 1). We present ZFT, ZHe and (U-Th)/He detrital apatite (AHe) data to resolve the thermal history of the IBSR and investigate the underlying causes that contributed to the heating and cooling along the India-Asia collision zone in NW India.

2. Geologic Background

2.1 Tectonic Setting

From south to north, the India-Asia collision zone in NW India (Figure 1) is composed of: a) the Precambrian–Paleocene Greater Indian passive margin metasedimentary and sedimentary rocks of the Tethyan Himalaya with an isolated klippe of the Cretaceous Spongtang oceanic arc (Garzanti et al., 1987; Buckman et al., 2018), b) the Indus Suture Zone containing the Lamayuru Complex – the Mesozoic deep-water slope facies of the Indian margin (Robertson and Sharp,

1998), and the Dras-Nidar Complexes – an assemblage of Cretaceous ophiolitic mélange, volcanic and volcano-sedimentary units (Ahmad et al., 2008; Walsh et al., 2019), c) the Late Cretaceous-Pliocene IBSR (Garzanti and Van Haver, 1988; Searle et al., 1990), and d) the southern edge of the Early Cretaceous–Early Eocene Ladakh batholith (Weinberg and Dunlap, 2000). The IBSR unconformably overlies the Ladakh batholith to the north and are in fault contact with the Dras-Nidar Complexes to the south (Figure 1; Searle et al., 1990; St-Onge et al., 2010). Pre-collisional deposition of the IBSR initiated in an arc-bounded or forearc marine basin in Late Cretaceous time, and the depocenter evolved into a continental intermontane basin with the onset of India-Asia collision in Early Eocene time (Garzanti and van Haver, 1988; Henderson et al., 2010). Regional IBSR deposition largely ended by Late Oligocene–Early Miocene time (~26–23 Ma) when basin inversion began, although local-scale deposition continued in Pliocene time in patches of western and central Ladakh (Mathur, 1983; Clift et al., 2002, Henderson et al., 2010, 2011).

Structurally, the IBSR constitutes the footwall of the regional north-vergent Main Zanskar backthrust (Searle et al., 1997), also known as the Great Counter thrust (GCT, Figure 1). Multiple strike-parallel, north-vergent thrusts belonging to the GCT system deform the IBSR (Steck, 2003). The timing of movement along the GCT in NW India is indirectly constrained to 23–20 Ma on the basis of the age of tectonic and metamorphic processes in the Himalayan orogen. Using $^{40}Ar/^{39}Ar$ hornblende ages, Searle et al. (1992) determine that peak metamorphism (700–750 °C, 8 kbar) and maximum crustal thickening in the Zanskar Himalaya (Fig. 1) south of the GCT occurred at ~28–23 Ma. Sinclair and Jaffey (2001) and Clift et al. (2002) suggest that this episode of crustal thickening and uplift in the Himalayan wedge at ~28–23 Ma provided the mechanical force to initiate movement along the GCT at ~23–20 Ma, thereby inverting the IBSR. Recent studies from south Tibet, based on detrital geochronology-thermochronology datasets and cross-cutting

relationships among Neogene intrusive rocks, also indicate that motion along the GCT initiated at ~23 Ma and largely ended by ~15 Ma (Zhang et al., 2011; Carrapa et al., 2014; Laskowski et al., 2018; Orme, 2019).

2.2 Stratigraphy

The IBSR stratigraphy comprises two major rock groups (Table 1, Figures 1, 2A-C): (a) the southern Late Cretaceous–Early Eocene marine Tar Group (Figures 2B-C), and (b) the northern Early Eocene to Pliocene continental Indus Group (Figure 2A-C). The Tar Group consists of carbonate and siliciclastic rocks that are tectonically bounded to the south by the pre-collisional Dras-Lamayuru-Nidar Complexes and are juxtaposed in the north against the Indus Group. The Indus Group exhibits extreme along-strike variations in siliciclastic fluvial facies that unconformably overlie the Ladakh batholith (Brookfield and Andrews-Speed, 1984; Garzanti and Van Haver, 1988; Searle et al., 1990; Sinclair and Jaffrey, 2001; Clift et al., 2002; Steck, 2003; Wu et al., 2007; St-Onge et al., 2010; Henderson et al., 2010, 2011; Tripathy-Lang et al., 2013; Singh et al., 2015). The Indus Group is categorized into two sub-groups: (i) the Early Eocene–Early Miocene Lower Indus Group and (ii) the Pliocene Upper Indus Group. The former is regionally present along the India-Asia collision zone, while the latter is localized to central and far-western Ladakh (Mathur, 1983; Henderson, et al., 2010).

2.3 Previous Low-temperature Thermochronometric Studies

Low-temperature thermochronologic data and other thermal proxies from the IBSR are limited to a few local studies with conflicting interpretations, leaving the regional thermal history undetermined. K/Ar mica ages from phyllites of the Indus Basin indicate a low-grade anchizonal metamorphic event along its southwestern margin in Middle–Late Eocene time, when fold-thrust

deformation occurred in the Tethyan Himalaya (Van Haver et al., 1986; Steck, 2003). Using illite crystallinity and vitrinite reflectance, Van Haver (1984) determined peak basin temperatures of ~280 °C in the uppermost Tar Group (Nummulitic Limestone Formation, Figure 2B) and ~155 °C in the Lower Indus Group. Clift et al. (2002) report 14–12 Ma AFT ages from two Lower Indus Group samples and interpret that these ages reflect cooling following basin inversion owing to regional counterthrusting along the GCT at ~23–20 Ma. An illite crystallinity estimate by Clift et al. (2002) in central Ladakh suggests temperatures did not exceed 200 °C in the Indus Group. Another paleo-geotemperature study from the Indus Group in eastern Ladakh by Schlup et al. (2003), which is also discussed in Clift et al. (2004), reveals an illite crystallinity index of 0.36 (°Δ2θ). This illite crystallinity value translates to a lower anchizone grade burial temperature of ~239°C using the index-temperature equation of Zhu et al. (2016). Schlup et al. (2003) also report a ZFT central age of 23 ± 2 Ma and an AFT age of 7.4 ± 0.7 Ma on a single Lower Indus Group sandstone sample. The 23 ± 2 Ma ZFT age is interpreted to reflect source cooling and is attributed to the exhumation of the Ladakh batholith, while the 7.4 ± 0.7 Ma AFT age suggests post-depositional cooling in the basin. Tripathy-Lang et al. (2013) report unreset ZHe ages of ~52–28 Ma in the Lower Indus Group Late Oligocene Basgo Formation and attribute them to the exhumation of source regions on the Indian plate.

3. Sampling and Analytical Methods

3.1 Sampling

We sampled medium-grained sandstones from four N-S to NNE-SSW trending sections across the IBSR in central Ladakh (Figures 1, 2A-C). These sections include: a) Temesgam (Figure 2A), b) Basgo, (Figure 2A), c) Zanskar Gorge (Figure 2B) and d) Upshi-Lato (Figure 2C). We collected eight samples from the Zanskar Gorge for ZFT analyses (Figure 2B). Low yield of good

144 quality dateable apatite in most samples and zircon in several samples limited our overall AHe
145 (two samples; Figures 2A, 2C) and ZHe datasets (six samples; Figures 2A-C).

146 Zircon and apatite concentrates were separated from each 8-10 kg sample using
147 conventional mineral separation techniques involving a rock crusher, water table, Frantz magnetic
148 separator and heavy liquids. Only samples DZA23TM from the Temesgam Formation (Figure 2A)
149 and DZA08UL (Figure 2C) from the Lower Upshi Formation produced apatites suitable for AHe
150 dating. Zircon yield in DZA08UL was low.

151 3.2. Zircon fission-track thermochronology

152 The zircons were mounted, polished and etched with KOH–NaOH at 220 °C for 12–36
153 hours following standard procedures of the London Fission Track Research Group. Mounts were
154 then irradiated with muscovite external detectors and dosimeter glass CN-5 and CN-2 at the
155 thermal neutron facility of the Risø reactor, Denmark. Fission-track densities were measured using
156 an optical microscope at 1250x magnification with an oil objective. Ages (±1σ) were calibrated by
157 the zeta method (Hurford and Green, 1983), using a zeta factor of 127 ± 5 for zircon determined
158 by multiple analyses of zircon standards following the recommendations of Hurford (1990).

159 ZFT ages indicate cooling through the 240 ± 40 °C temperature window depending on their
160 U-concentrations (Hurford, 1986). Ideally, if all the ZFT ages are younger or older than
161 depositional age of the basin, they indicate cooling in the basin or source, respectively. A mixture
162 of older and younger ages, spanning pre- and post-deposition ages, likely suggests a case of partial
163 fission-track annealing (or partial resetting) in zircon that indicates basin temperatures were within
164 240±40 °C. Partial annealing of zircon fission tracks begin at ~185–200 °C and the annealing is
165 complete above ~280–300 °C (Bernet and Garver, 2005).

3.3 (U-Th)/He Zircon and Apatite Thermochronology

At the Arizona Radiogenic Helium Dating Laboratory, 3–5 mostly inclusion-free zircon and apatite grains with angular crystal faces were hand-picked from each sample (if available) and packed into Nb tubes. Applying the standard procedures of He extraction using coupled laser heating, the He content was measured on a quadrupole mass spectrometer, and subsequent Th and U contents were measured using ICP-MS following the methods of Reiners (2005). Raw ages were obtained by solving the combined radioactive decay-diffusion equation with known analytical concentrations of U, Th and He; raw ages were corrected by applying the alpha-ejection protocols of Farley et al, (1996). If the ZHe and AHe ages are younger than the depositional age of the formation, this implies basin burial temperatures of >140–200 °C and >40–90 °C, respectively, and the ages are interpreted as thermally reset. ZHe or AHe ages that are older than the depositional age of the sample are unreset and reflect cooling of the source before deposition.

3.4 Thermal Modeling

The ZHe and AHe ages from each sample were inverse modelled in the thermal modeling program HeFTy v.1.9.1 (Ketcham, 2005) to determine the time-Temperature (*t*-*T*) paths using the diffusion model of Guenthner et al. (2013). The forward model in HeFTy predicts the expected grain age data distribution for a given *t*-*T* path. The inverse algorithm solves for a family of *t*-*T* paths that a sample could have experienced for a fixed input dataset that include cooling ages, U-Th-Sm concentrations, grain size and zonation parameters. For each resultant *t*-*T* path, HeFTy calculates the statistical fit between measured and the predicted cooling ages. Acceptable-fit paths have a Kolmogorov-Smirnov probability ≥ 0.05, while good-fit paths have a Kolmogorov-Smirnov probability ≥ 0.5. A weighted mean path and a best-fit *t*-*T* path is also generated from the inversion process. The weighted mean path is an overall summary of the inversion process with weights

189 based on the goodness of fit statistics associated with the acceptable and good-fit paths; it may or
190 may not have an acceptable or a good fit to the data. The best-fit path has the highest goodness of
191 fit and represents the most reasonable thermal history of a sample under the assigned constraints.

192 **4. Results**

193 Our ZFT, ZHe, and AHe results are summarized in Table 2 and Figure 3 (data available in
194 the Supplementary File, Sections A–D). All ages are reported at 1σ uncertainty level. For previous
195 studies that used the youngest single grain age (e.g., youngest single detrital zircon or muscovite
196 grain age) to constrain the maximum depositional ages (MDAs) of a unit, we recalculated the
197 MDA by estimating the weighted mean age of the youngest cluster with overlapping uncertainties
198 (i.e., YC1σ(2+) and YC2σ(3+) ages; Table 2, Dickinson and Gehrels, 2009). If true depositional
199 age (e.g., biostratigraphic or geochronologic tuff ages) is not available for a formation, the
200 YC2σ(3+) age is adopted as a conservative estimate of its MDA (Coutts et al., 2019). Therefore,
201 unless specified, a MDA reported in this study refers to the YC2σ(3+) age, which is the weighted
202 mean age of the youngest cluster of 3 or more grains with overlapping 2σ uncertainties.

203 The individual ZFT ages span from Cretaceous to Middle Miocene time, 182.15 ± 50.20 –
204 13.95 ± 2.98 Ma. Although the objective was to date 50–100 grains per sample for ZFT, low yield
205 of zircon resulted in 17–65 grains per sample. All eight samples from the Zanskar Gorge (Figures
206 2B, 3A) fail the χ^2 test ($P(\chi^2) < 5\%$) indicating the presence of some overdispersion amongst the
207 population of measured grain ages. However, levels of overdispersion expressed as % dispersion
208 of the central age are not always high, suggesting that in some cases, the overdispersion is not
209 significant or poorly developed in terms of defining discrete age components. The ZFT data were
210 decomposed into statistical grain-age components or modes using RadialPlotter (Vermeesch,
211 2009; Table 2); however, these do not necessarily capture the true age modes if represented by

only a few grains. In some cases, a few higher precision ages may be identified as an age mode rather than a population of grains that capture the true Poisson age distribution. To help determine the significance of the component ages, the data are also plotted as Abanico diagrams that combine a radial plot and a probability density estimate (Supplementary File, section B). These plots help to visualize the distribution of ages in each sample in terms of age modes or groups, like the youngest age mode, the secondary age mode and the oldest age mode.

The individual ZHe ages are all Miocene, 19.04 ± 0.54 – 8.57 ± 0.11 Ma (Table 2, Figure 3B). The AHe ages are Late Miocene–Pliocene, 6.77 ± 0.40 – 3.94 ± 0.17 Ma (Table 2, Figure 3B).

5. Interpretations

5.1 Tar Group and Lato Formation

The Tar Group, which has a biostratigraphically-determined depositional age limit of ~55–50 Ma (Green et al., 2008; Henderson et al., 2010), is partially reset with respect to the ZFT system, with ages from Zanskar Gorge yielding 130.92 ± 31.87 to 21.53 ± 4.61 Ma for the lowermost Jurutze Formation (sample ZG45), 76.79 ± 14.40 to 13.95 ± 2.98 Ma for the Chogdo Formation (sample ZG55) in the middle, and 182.15 ± 50.20 to 22.60 ± 4.57 Ma for the topmost Nummulitic Limestone Formation (sample ZG62). The zircon populations (or modes), which are younger than the depositional ages in Chogdo (ZG55) and Nummulitic Limestone (ZG62) Formations confirm partial resetting (Table 2, Figure 3A). Although sample ZG45 from the Jurutze Formation contains a single mode of 65.2 ± 3.1 Ma, which is older than its 54.7 ± 0.3 Ma U-Pb detrital zircon MDA (Table 2), this ZFT age likely reflects partial resetting within the PAZ whereby the older, inherited zircons within the Jurutze Formation were not thermally reset to take them below the MDA. Our

data suggest that the burial temperatures in the Tar Group exceeded the ZFT lower partial annealing temperatures of ~185-200 °C. However, basin temperatures did not exceed the higher annealing temperatures of ~280-300 °C above which ZFT ages are completely reset.

The ZHe ages from the Tar Group Sumdo Formation (DZT20ZV; 15.42 ± 0.20 - 8.57 ± 0.11 Ma) in the Zanskar Gorge are all younger than its biostratigraphic age of ~55-51 Ma (Henderson et al., 2010), indicating post-depositional temperatures exceeded 180-200 °C (Table 2, Figure 3B). The Lato Formation (possibly Cretaceous in age) within the Upshi-Lato transect is older than the youngest units of the Tar Group and has ZHe ages (DZA12UL; 12.62 ± 0.26 - 10.05 ± 0.20 Ma) that are all considerably younger than its stratigraphic age (Table 2, Figure 3B). Therefore, the Lato Formation is also reset.

5.2 Indus Group

In the Lower Indus Group at Zanskar Gorge, the 50.3 ± 3.3 Ma ZFT modal age of the Nurla Formation (sample ZG42) is within error of its U-Pb detrital zircon MDA of ~51 Ma (Table 2, Figure 3A; Bhattacharya, 2020). Stratigraphically overlying the Nurla Formation, the Choksti Conglomerate (sample ZG38), which is the basal member of the Choksti Formation, has two ZFT modes, 40.3 ± 2.1 and 68.6 ± 4.1 Ma (Table 2, Figure 3A). These two age modes are approximately equal to or older than the U-Pb detrital zircon MDA of the Choksti Formation, which is 41.5 ± 0.2 Ma (Wu et al., 2007). The Upper Choksti member (sample ZG30), which is the topmost member of the Choksti Formation, has four ZFT modes: 26.6 ± 2.2 Ma (M1), 37.8 ± 3.8 Ma (M2), 49.5 ± 4.4 (M3) and 83 ± 8.4 Ma (M4; Table 2, Figure 3A). The Upper Choksti Member is stratigraphically correlatable to the Hemis and Lower Upshi Formations and the latter have U-Pb detrital zircon MDAs of 37.8 ± 0.2 Ma and 38.3 ± 0.2 Ma, respectively (Table 2; Sinclair and Jaffey, 2001; Henderson et al., 2011; Bhattacharya, 2020). The Choksti Formation is also older

than the Basgo Formation, which has a Late Oligocene biostratigraphic age (Bajpai et al., 2004; Tripathy-Lang et al., 2013). The M1 mode of Upper Choksti is thus younger than its depositional age, reflecting partial resetting of sample ZG30. Interestingly, partial resetting is not detected in samples ZG42 and ZG38 from the underlying Nurla Formation and Choksti Conglomerate member. This is because these two samples probably contained older zircon populations, which remained above their corresponding MDAs, despite partial resetting. The youngest M1 mode from the Lower Nimu Formation (sample ZG21) is 25.5 ± 3.1 Ma, which is younger than its $^{40}Ar/^{39}Ar$ detrital muscovite MDA of 32.3 ± 0.2 Ma. In terms of true depositional age, the Lower Nimu Formation is at least older than the biostratigraphically-dated Late Oligocene Basgo Formation (Bajpai et al., 2004; Buckman et al., 2018). The M1 mode of the Lower Nimu Formation thus indicates partial resetting. The upper Indus Group Upper Nimu Formation (ZG16) is unreset, with ZFT modes older than its corresponding $^{40}Ar/^{39}Ar$ detrital muscovite MDA of 9.5 ± 0.5 Ma (Table 2, Henderson et al., 2010). Overall, like the Tar Group, the Lower Indus Group is also partially reset with respect to the ZFT system, whereas the Upper Indus Group is unreset.

Along the Upshi-Lato traverse, the Lower Indus Group Lower Upshi Formation (sample DZA09UL) has ZHe ages from 17.79 ± 0.26 – 13.63 ± 0.21 Ma (Table 2, Figure 3B). The Lower Upshi Formation and its stratigraphically correlatable Hemis Formation both have detrital zircon and muscovite MDAs of ~38 Ma (Table 2; Henderson et al., 2011; Bhattacharya, 2020). The ZHe ages in the Lower Upshi Formation are thus younger than its inferred MDA. Along the Basgo traverse, the Lower Indus Group Basgo Formation (sample DZA07SA) ZHe ages are from 19.04 ± 0.54 – 9.90 ± 0.27 Ma, which are younger than its ~28–26 Ma true depositional age based on ostracods (Bajpai et al., 2004). From the Temesgam traverse, the Lower Indus Group Temesgam Formation (sample DZV23TM) exhibits ZHe ages from 18.91 ± 0.52 – 12.81 ± 0.18 Ma, which

are younger than its U-Pb detrital zircon MDA of 26.8 ± 0.1 Ma (Table 2; Bhattacharya, 2020). The AHe ages from the Lower Upshi Formation (sample DZA08UL; 6.56 ± 0.10 – 5.22 ± 0.30 Ma) and the Temesgam Formation (sample DZV23TM; 6.77 ± 0.40 Ma – 3.94 ± 0.17 Ma) are younger than their corresponding ZHe ages (Table 2; Figure 3B).

All ZHe ages from the Lower Indus Group are <20 Ma. Deposition in the Lower Indus Group of central Ladakh ended by ~26–23 Ma, after which basin inversion and regional counterthrusting began at ~23–20 Ma (Clift et al., 2002; Bhattacharya, 2020). Therefore, we interpret the ZHe and AHe ages from the Lower Indus Group formations as thermally reset. This is consistent with our earlier interpretation that the Lower Indus Group is partially reset with respect to the ZFT system, implying peak burial temperatures exceeded 185–200 °C but stayed below 280–300 °C. By contrast, the stratigraphically youngest Upper Indus Group Upper Nimu Formation yields ZHe ages (sample DZA17ZV; 17.39 ± 0.35 – 13.70 ± 0.27 Ma) older than its corresponding $^{40}Ar/^{39}Ar$ detrital muscovite MDA of 9.5 ± 0.5 Ma (Henderson et al., 2010). The Upper Indus Group is therefore unreset with respect to the ZHe system (Table 2, Figure 3B).

No correlation exists between ZHe or AHe ages and grain size in individual samples. However, compilation of all the ZHe ages reveals a moderate positive correlation between age and grain size, which may contribute to the inter-sample ZHe age dispersion (Supplementary File, Section E). No correlation exists between AHe ages and grain size. Overall, no correlation is observed between effective uranium and ZHe or AHe ages within individual samples or collectively (Supplementary File, Section E). This suggests that radiation damage is not the primary influence of intra-sample ZHe and AHe age variability and the distribution of ZHe ages are largely geologically controlled. The only exception is sample DZA07SA from the Basgo Formation, which shows strong negative correlation between ZHe age and effective uranium (R^2

303 = ~0.7) suggesting some control of radiation damage on the observed cooling ages (Supplementary
304 File, Section E).

305 **6. Thermal modeling of (U-Th)/He cooling ages**

306 6.1 Modeling Strategy

307 Using our ZHe and AHe data in the thermal modeling program HeFTy, we tested two *t-T*
308 modeling approaches to determine the cooling history of the Indus Basin rock samples. The first
309 approach involves considering post-depositional *t-T* constraints based on known regional geologic
310 information, while the second approach lacks any specific post-depositional *t-T* constraints. The
311 purpose of testing the second approach was to check if we can reproduce near-identical cooling
312 histories without imposing particular post-depositional *t-T* constraints in the models thus reducing
313 bias.

314 Indus Basin sedimentation began in Late Cretaceous time with the deposition of the marine
315 Tar Group, which continued until ~50 Ma (Henderson et al., 2010). After ~50 Ma, the continental
316 facies of the Lower Indus Group were deposited until Late Oligocene–Early Miocene time
317 (Sinclair and Jaffey, 2001; Clift et al., 2002; Henderson et al., 2011). The Indus Basin was inverted
318 at ~23–20 Ma (Clift et al., 2002) and there is no prior evidence of post-depositional basin cooling.
319 In our first approach, to fit the ZHe and AHe data in the context of known regional geologic
320 information, we allow individual models to explore the *t-T* space younger than 23 Ma and colder
321 than 240 or 280 °C (whichever applicable; Figures 4A-E). We apply surface depositional
322 temperatures of 0–25 °C and let all the models solve for *t-T* paths from temperatures greater than
323 the closure temperature window of the warmest thermochronometric system modelled. The ZFT,
324 ZHe, and AHe partial annealing/retention temperatures considered are 240 ± 40 °C (Hurford,

1986), 140–200 °C (Reiners, 2005; Guenthner et al., 2013), and 40–90 °C (Ehlers and Farley, 2003), respectively. Based on the knowledge of regional thermal history, a temperature constraint of 0–280 °C was applied only to the Sumdo Formation (Sections 2.3, 6.1.2), while a 0–240 °C constraint was imposed on the *t-T* models of the Lato, Lower Upshi, Basgo and Temesgam Formations (Sections 6.1.1, 6.1.3–6.1.5). The input *t-T* constraints are shown by hollow rectangle boxes in Figures 4A-E and are detailed for each formation in sections 6.1.1–6.1.5. For a given sample, simultaneous modelling of individual ZHe ages, or a mix of individual ZHe and AHe ages (2–3 grains or more), yielded no good or acceptable paths with the known input data. This is a common problem with HeFTy as noted in multiple previous studies (e.g., Carrapa et al., 2014); the program could not satisfy all input parameters for a single sample simultaneously and produce acceptable results. Therefore, mean ZHe and AHe ages were calculated and incorporated as input data for *t-T* model extraction in HeFTy using the diffusion model of Guenthner et al. (2013). Inverse modeling produced a set of possible *t-T* paths for a given sample based on the user assigned *t-T* constraints. We ran the models until at least 100 good fit *t-T* paths were generated. The best fit *t-T* path of each model represents a statistically robust thermal history of the corresponding sample (Figures 4A-E).

In the second approach of *t-T* modeling, we constrain the depositional age of the sample and its surface depositional temperatures (0–25 °C); this allows HeFTy to explore maximum area in the post-depositional *t-T* space and generate a family of *t-T* paths that do not depend on known geologic information from the region. Similar to first approach, at least 100 good fit *t-T* paths were produced (Supplementary File, Section F). Although the best-fit *t-T* paths from our second approach show cooling beginning approximately within the same age range as in the first approach, not all the resultant *t-T* paths yield a geologically meaningful thermal history. Several acceptable

and good-fit paths demonstrate *t-T* histories that are unrealistic considering the available data on the timing of basin sedimentation, burial, inversion and cooling. Not all statistically acceptable or good-fit *t-T* paths obtained in our second approach are thus representative of the post-depositional cooling history of the basin. We examine the causes of rejection for individual models in Supplementary File, Section F. The second approach is not discussed henceforth and the following sub-sections 6.1.1-6.1.5 focus on the *t-T* constraints imposed by regional geologic data as per the first approach.

6.1.1 Lato Formation

The Indian margin unit Lato Formation was deposited on the surface at 0–25 °C in possibly Cretaceous time (Figure 4A). The Lato Formation is speculated to be correlatable to the Mesozoic Lamayuru Complex or the Mesozoic Chilling Formation in the Zanskar Gorge (Henderson et al., 2011), both of which are Indian margin units that are older than Early Eocene. Henderson et al. (2011) obtained two ~51 and ~77 Ma U-Pb detrital zircon grain ages and a ~67 Ma $^{40}Ar/^{39}Ar$ detrital muscovite grain age from the Lato Formation; all other detrital grains are >350 Ma. The 3 youngest grain ages do not overlap within 2σ; therefore, instead of taking a weighted average, we consider the ~77 Ma grain age as a conservative estimate of MDA for the Lato Formation. The Lato Formation is older than, or coeval with, the youngest Tar Group units that were deposited between 55 and 50 Ma (Henderson et al., 2010, 2011). Therefore, in our HeFTy model, we constrain the depositional age of the Lato Formation from ~77-50 Ma, which is consistent with regional stratigraphic correlations.

Cooling is constrained through 0–240 °C after ~23 Ma. Despite being older than the Tar Group, there is no evidence of burial temperatures exceeding 240 °C in the Lato Formation, and the depositional setting of the Lato Formation relative to Tar Group is undetermined. The Tar

371 Group, which experienced temperatures >240 °C, has blue-grey phyllite (Van Haver, 1984; Clift
372 et al., 2002; Henderson et al., 2010) and was probably deposited just north of the Lato Formation
373 that contains relatively unaltered sandstone.

374 6.1.2 Sumdo Formation

375 The Tar Group Sumdo Formation was deposited at the surface (0–25 °C) at ~55–51 Ma
376 (Figure 4B; Henderson et al., 2010). ZFT ages from the overlying Chogdo Formation and the
377 underlying Jurutze Formation are partially reset, which suggest peak burial temperatures between
378 200–280 °C in the Sumdo Formation. Van Haver (1984) calculated a maximum burial temperature
379 of ~280 °C using illite crystallinity from the overlying Nummulitic Limestone Formation.
380 Therefore, we constrain cooling after 23 Ma through 0–280 °C.

381 6.1.3 Lower Upshi Formation

382 The Lower Indus Group Lower Upshi Formation (Figure 4C) is correlatable to the Hemis
383 Formation, and both have detrital zircon and muscovite MDAs of ~38 Ma (Henderon et al., 2011;
384 Singh et al., 2015; Bhattacharya, 2020). The $^{40}Ar/^{39}Ar$ detrital muscovite MDA of the Upper Upshi
385 Formation, which overlies the Lower Upshi Formation, is ~25 Ma (Table 2; Henderson et al.,
386 2011). Because true depositional ages can be younger than MDAs, we relax the depositional age
387 for the Lower Upshi Formation in our HeFTy model to be from ~38–23 Ma. The upper age of ~23
388 Ma is based on the ~26–23 Ma cessation of Lower Indus Group deposition in central Ladakh, after
389 which regional counterthrusting began at ~23–20 Ma (Clift et al., 2002; Bhattacharya, 2020). Our
390 ZFT results indicate that the Lower Indus Group is partially reset with respect to the ZFT system,
391 indicating peak burial temperatures >185–200 °C. In addition, paleo-geotemperature estimates
392 from the Lower Indus Group based on illite crystallinity also suggest maximum burial

393 temperatures of ~239°C (Schlup et al., 2003; Clift et al., 2004). Hence, we allow the model to cool
394 through 0–240 °C after ~23 Ma.

395 6.1.4 Basgo Formation

396 The Lower Indus Group Basgo Formation is ~10–200 m thick (Garzanti and Van Haver,
397 1988) and is biostratigraphically dated as Late Oligocene in age (Bajpai et al., 2004) with a ~27
398 Ma youngest single zircon MDA (Bhattacharya, 2020). The Basgo Formation is conformably
399 overlain by the Temesgam Formation, which was deposited from 26–23 Ma (Bhattacharya, 2020).
400 In our *t-T* model, we constrain the depositional age of the Basgo Formation at ~28–26 Ma (Figure
401 4D). Because Lower Indus Group temperatures did not exceed 240 °C, we constrain model cooling
402 through 0–240 °C after ~23 Ma.

403 6.1.5 Temesgam Formation

404 The Lower Indus Group Temesgam Formation has a U-Pb detrital zircon MDA of ~27 Ma
405 and was deposited conformably on top of Basgo Formation from 26–23 Ma (Table 2,
406 Bhattacharya, 2020). Therefore, in our *t-T* model, we constrain the depositional age of the
407 Temesgam Formation from ~26–23 Ma (Figure 4E). An upper age limit of ~23 Ma is imposed
408 from the estimated age of inversion of the Indus Basin (Clift et al., 2002). Like other Lower Indus
409 Group Formations, we allow model cooling through 0–240 °C after 23 Ma.

410 6.2 Model Results

411 All the *t-T* models demonstrate cooling from above or within the ZHe partial retention zone
412 temperatures of 140–200°C through at least 100 good and ≥188 acceptable paths (Figures 4A–E).
413 The best-fit *t-T* model paths show the onset of cooling by ~22–20 Ma in the Lower Indus Group
414 Lower Upshi, Basgo and Temesgam Formations (Figures 4C–E), and by ~15–13 Ma in the Lato

and Sumdo Formations (Figure 4A–B). It is possible that cooling may have started earlier than the time indicated by the best-fit *t-T* paths in the Lato and Sumdo Formations as well; a number of good-fit paths in each model suggest cooling began before ~15–13 Ma (Figures 4A–B). We interpret the time of initiation of cooling along the best-fit *t-T* path as the minimum time by which cooling was onset in the sample. The best-fit model paths for the Indian margin Lato Formation and the Tar Group Sumdo Formation, demonstrate a peak burial temperatures (235–245 °C) well exceeding the maximum ZHe partial retention zone temperature of ~200 °C, suggesting that the Lato and Sumdo Formations are reset and the ZHe ages reflect post-depositional basin cooling (Figures 4A–B). The Lower Upshi, Basgo and Temesgam Formations are likely reset as well; the best-fit *t-T* model paths record cooling from above 170–190 °C, which indicate burial within the higher side of the ZHe partial retention zone. We would like to remind here that our *t-T* modeling is a consequence of using mean ages in each model. If individual ZHe ages are modelled grain by grain, it does not significantly change the results determined by using mean ages, and best-fit paths still indicate cooling beginning between ~22 and 11 Ma. In summary, the *t-T* modeling results presented in this study confirm the presence of a post-depositional cooling signal in the Indus Basin beginning at ~22–20 Ma, and show that burial temperatures in the Indian margin Lato Formation, Tar Group and the Lower Indus Group exceeded 170–190 °C.

7. Discussion

7.1 Post-depositional Thermal Evolution of the IBSR

In general, the IBSR in central Ladakh, excluding the Upper Indus Group, experienced a post-depositional Miocene–Pliocene cooling phase from >170–200 °C. The ZFT results suggest that post-depositional peak basin temperatures exceeded 185–200 °C in the Tar and Lower Indus Groups but stayed below 280–300 °C (Table 2). This basin heating resulted in partial resetting of

438 the Tar and Lower Indus Group rocks with respect to the ZFT system. Our ZFT age interpretations
439 are consistent with the 280 °C and 240 °C maximum burial temperatures of the Tar and Lower
440 Indus Group rocks determined using illite crystallinity and/or vitrinite reflectance (Van Haver,
441 1986; Schlup et al., 2003, Clift et al., 2004). Although the best-fit (U-Th)/He *t-T* model paths from
442 the Lower Indus Group suggest burial temperatures of ~170–190 °C, this is likely a consequence
443 of relative extent of burial in the sampled sections. The Zanskar section, from where our ZFT
444 samples are collected, exposes more altered sandstones (Tripathy-Lang et al., 2013) compared to
445 the Upshi-Lato, Basgo, and Temsgam sections, from where our Lower Indus Group ZHe and/or
446 AHe samples are collected.

447 Our ZHe age data range between ~19 and 8 Ma (Table 2, Figure 3B); however, these ages
448 alone cannot be used to estimate when basin cooling began. Thermal modeling results suggest that
449 cooling initiated by ~22–20 Ma in the Lower Indus Group of the Indus Basin (Figures 4C–E) and
450 was occurring throughout the basin by ~15–12 Ma (Figures 4A–B). The majority of the ZHe
451 cooling ages are between ~16 and 10 Ma, and all our thermal models demonstrate steady or rapid
452 cooling through 200–140 °C between ~20 and 10 Ma (Figure 4). Therefore, we suggest that
453 cooling largely occurred through ZHe temperatures in Early–Middle Miocene time. Cooling
454 continued into the Pliocene time until at least ~4 Ma, which is supported by our ~7–4 Ma AHe
455 cooling ages and model paths (Table 2, Figure 4). Our interpretation expands the ~14–7 Ma post-
456 depositional cooling phase previously identified in the Lower Indus Group using three AFT central
457 ages (Clift et al., 2002; Schlup et al., 2003). It is also possible that the timing of initiation of cooling
458 decreases from north to south across the basin. For example, cooling may have begun earlier in
459 the northern Lower Indus Group Formations between ~22 and 20 Ma (Figures 4C–E), and then
460 progressed southwards in the Tar Group and Lato Formation between ~15-12 Ma (Figures 4A–B);

however more low-temperature thermochronometric studies are required in the region to check for such age trends across the Indus suture. Overall, this study in the Indus Basin of central Ladakh reveals a post-depositional Miocene–Pliocene cooling phase (~22–4 Ma) that initiated at ~22–20 Ma.

Unreset ~17–14 Ma ZHe ages from the Pliocene Upper Nimu Formation (Table 2; Mathur, 1983; Henderson, 2010) of the stratigraphically youngest Upper Indus Group indicate post-depositional basin temperatures <140 °C. The Upper Indus Group is ~1 km thick (Henderson et al., 2010); therefore, Pliocene deposition of the Upper Indus Group did not influence the cooling of either the Tar Group or the Lower Indus Group.

7.2 Cause of Basin Burial: Sedimentation or Overthrusting

In the Indus Basin, peak burial temperatures exceeded 170–190 °C just before cooling began between ~22 and 20 Ma (Figure 4A–E). This requires the IBSR, excluding the Upper Indus Group, to be progressively buried by sedimentation and/or regional overthrusting. Stratigraphic studies indicate at least ~4.5 km of sediment was deposited in the Indus Basin by Early Miocene time (Henderson et al., 2010; Bhattacharya, 2020), which suggests some of the basin heating was the result of this stratigraphic overburden (assuming a geotherm of 20–30 °C/km). We suggest that additional burial was caused by regional overthrusting associated with the GCT. Although the age of the GCT is not well constrained by geochronological methods in NW India, it is thought to have initiated in Early Miocene time at ~23–20 Ma (Sinclair and Jaffey, 2001; Clift et al., 2002; discussed in Section 2.1). Kirstein et al. (2009) support a >20 Ma age for the GCT that led to the burial of the southern edge of the Ladakh batholith. Recent studies from south Tibet also assert that the slip on the GCT initiated at ~23 Ma (Laskowski et al., 2018), and ceased by ~15 Ma in most locations (Zhang et al., 2011; Carrapa et al., 2014; Laskowski et al., 2018; Orme, 2019).

7.3 Implications and causes of cooling

Despite the relatively limited scope of our data, this is the first regionally extensive multi-thermchronometric study from the IBSR and reveals a post-depositional Miocene–Pliocene cooling event along the India-Asia collision zone in NW India. Deposition continued regionally along the collision zone until Late Oligocene–Early Miocene time (~26–23 Ma; Sinclair and Jaffey, 2001; Clift et al., 2002), and there is no unequivocal evidence of cooling beginning in the IBSR until ~22–12 Ma. Using the ZHe and AHe datasets, we calculate the amount of material removed since the onset of cooling at ~22–20 Ma. This requires assuming a paleo-geothermal gradient, which is challenging considering the few studies along the collision zone in NW India. Thermal modeling of ZFT and AFT ages in Kohistan, >350 km west of the study area, reveal Miocene geothermal gradients of ~40 °C/km (Zeitler, 1985). Based on the geothermal gradient calculated by Zeitler (1985), Sinclair and Jaffey (2001) bracket a 30–50 °C/km range for Miocene geothermal gradients in the Indus Basin to estimate exhumation rates of 0.10–0.40 mm/yr. However, a 30–50 °C/km geothermal gradient range is incompatible with recent studies from the region (e.g., Epard and Steck, 2008; Schlup et al., 2011; Langille et al., 2014; Kumar et al., 2017). Using a bootstrapping algorithm, Kumar et al. (2017) modelled a range of geothermal gradients from ~22–33 °C/km for the Early–Middle Eocene evolution of the Ladakh batholith (Figure 1) in NW India. In the Tso Morari Complex to the south (Figure 1), Eocene–Oligocene geothermal gradients were 18–22 °C/km, and the geothermal gradient has remained relatively unperturbed since 30 Ma (Epard and Steck, 2008; Schlup et al., 2011). East of the Tso Morari Complex, ~200 km south-east of the study area, Early Miocene geothermal gradients estimated from the Leo Pargil shear zone by analyzing the Barrovian metamorphic pressure-temperature paths vary from ~22–30 °C/km (Langille et al., 2014). Based on these neighboring geotherm estimates, we assume a

Miocene geothermal gradient of ~20–30 °C/km for the Indus Basin. It is essential to note that recent works from sedimentary basins along the India-Asia collision zone in south Tibet have all considered Miocene geothermal gradients within 20–30 °C/km (e.g., Carrapa et al., 2014; Li et al., 2016; Orme, 2019; Ning et al., 2019). Assuming a geothermal gradient of 20–30 °C/km, our ZHe cooling ages indicate cooling from a mean temperature of 204 °C requiring removal of at least ~7–10 km of rock since ~22 Ma.

A potential driver of the Miocene–Pliocene cooling is erosion by the Indus River, which has been draining the India-Asia collision zone in NW India since at least Early Miocene time (Sinclair and Jaffey, 2001; Henderson et al., 2010, 2011). Indus River erosion removed the GCT-overthrusted rocks that buried the Indus Basin, thereby resulting in the observed Miocene–Pliocene cooling. Although Indus River erosion played an important role in removing rocks from the India-Asia collision zone in Miocene–Pliocene time (e.g., Sinclair and Jaffey, 2001; Henderson et al., 2010), we cannot be certain that the river erosion was the primary factor triggering the onset of cooling between ~22 and 20 Ma. There is considerable debate as to whether the Indus River's flow along the suture zone began in NW India in Early Eocene or Early Miocene time (Searle et al., 1996; Sinclair and Jaffey, 2001; Clift et al., 2002; Najman, 2006; Henderson et al., 2010; 2011; Zhuang et al., 2015). If the Indus River first flowed along the suture zone in the Early Miocene, aggressive erosion resulting from its initiation may explain the onset of regional cooling. If the Indus River existed at this location since Early Eocene time, additional tectonic, geodynamic and geomorphological factors were also responsible for the initiation of cooling. Interestingly, along the Yarlung suture of the India-Asia collision zone in south Tibet, a regional Miocene cooling signal from ~21–7 Ma is well documented from low-temperature thermochronometric studies (e.g., Carrapa et al., 2014; Tremblay et al., 2015, Li et al., 2015, 2016, 2017; Ge et al., 2017; Orme,

2019). These studies generally attribute the Miocene cooling signal to GCT activity and/or Yarlung River erosion (Carrapa et al., 2014; Li et al., 2015, 2016, 2017; Ge et al., 2017; Orme, 2019), or intensification of Asian monsoon (Carrapa et al., 2014), while considering the regional uplift caused by the northward underthrusting of the Indian plate following Greater Indian slab break-off in Early Miocene time (DeCelles et al., 2011; Webb et al., 2017). Therefore, it is possible that, in NW India, a combination of tectonic, geodynamic, and geomorphological factors such as the aforementioned also resulted in a tectonic setting that facilitated regional cooling along the India-Asia collision zone in NW India. However, given the limited previously published and new data in this region, it is difficult to test such scenarios. This study therefore provides the foundation to investigate more complex tectono-thermal events in the India-Asia collision zone of NW India and test models that correlate them with the results from south Tibet.

8. Conclusions

Low-temperature thermochronology of the Indus Basin in central Ladakh reveals a post-depositional Miocene–Pliocene cooling history. Our ZFT and ZHe results confirm that the basin was buried to temperatures >170–200 °C and exceeded 240 °C in the deepest formations. Basin burial is attributed to sedimentation and regional northward counterthrusting by the GCT in Early Miocene time. Thermal modeling of ZHe and AHe ages indicate cooling onset by ~22–20 Ma, occurred rapidly or steadily across the basin through ZHe partial retention temperatures between ~20 and 10 Ma, and continued at least until ~4 Ma. This Miocene–Pliocene cooling, which removed ~7–10 km of rock from the India-Asia collision zone, may be linked to erosion by the Indus River that dissects the ISBR. However, more low-temperature thermochronometric data from western and eastern Ladakh are required to confirm if this cooling signal is present along the strike of the India-Asia collision zone in NW India, as documented in south Tibet. If a regional

Miocene–Pliocene cooling signal is indeed present both in NW India and south Tibet, it might be indicative of a continental-scale thermal event operating along the India-Asia collision zone driven by a combination of tectonic, geodynamic, and geomorphological factors rather than Indus river incision alone.

Acknowledgements

We thank the Editor-in-Chief, Dr. Taylor Schildgen for editorial handling and valuable feedback. Constructive reviews from Dr. Jean-Luc Epard and Dr. Ryan Leary greatly improved the manuscript. All thermochronological data are available in the Supporting Information file and are also being archived in the Geochron Data Repository in compliance with FAIR Data Standards. Student travel grants to GB by the Geological Society of America and The University of Alabama funded the fieldwork for this research. Uttam Chowdhury, Erin Abel and Peter Reiners at the Arizona Radiogenic Helium Dating Laboratory, The University of Arizona, assisted GB with the He-analyses. Talat Ahmad, University of Kashmir helped with procuring permits for fieldwork. Konchok Dorjay provided logistical support to GB in extreme weather conditions.

References

Ahmad, T., Tanaka, T., Sachan, H. K., Asahara, Y., Islam, R., & Khanna, P. P. (2008). Geochemical and isotopic constraints on the age and origin of the Nidar Ophiolitic Complex, Ladakh, India: Implications for the Neo-Tethyan subduction along the Indus suture zone. *Tectonophysics, 451*(1-4), 206-224. https://doi.org/10.1016/j.tecto.2007.11.049

Bajpai, S., Whatley, R. C., Prasad, G. V. R., & Whittaker, J. E. (2004). An Oligocene non-marine ostracod fauna from the Basgo Formation (Ladakh Molasse), NW Himalaya, India. *Journal of Micropalaeontology, 23*(1), 3-9. https://doi.org/10.1144/jm.23.1.3

Bhattacharya, G. (2020). Deposition, burial and cooling of the Indus Basin, Ladakh, northwest India: Implications for orogenic processes in the India-Asia collision zone. PhD Dissertation, The University of Alabama.

Bernet, M., & Garver, J. I. (2005). Fission-track analysis of detrital zircon. *Reviews in Mineralogy and Geochemistry, 58*(1), 205-237. https://doi.org/10.2138/rmg.2005.58.8

Brookfield, M., & Andrews-Speed, C. (1984). Sedimentology, petrography and tectonic significance of the shelf, flysch and molasse clastic deposits across the Indus suture zone, Ladakh, NW India. *Sedimentary Geology, 40*(4), 249-286. https://doi.org/10.1016/0037-0738(84)90011-3

Buchs, N., & Epard, J.-L. (2018). Geology of the eastern part of the Tso Morari nappe, the Nidar Ophiolite and the surrounding tectonic units (NW Himalaya, India). *Journal of Maps, 15*(2), 38-48. https://doi.org/10.1080/17445647.2018.1541196

Buckman, S., Aitchison, J. C., Nutman, A. P., Bennett, V. C., Saktura, W. M., Walsh, J. M. J., . . . Hidaka, H. (2018). The Spongtang Massif in Ladakh, NW Himalaya: An Early Cretaceous record of spontaneous, intra-oceanic subduction initiation in the Neotethys. *Gondwana Research, 63*, 226-249. https://doi.org/10.1016/j.gr.2018.07.003

Carrapa, B., Orme, D., DeCelles, P. G., Kapp, P., Cosca, M. A., & Waldrip, R. (2014). Miocene burial and exhumation of the India-Asia collision zone in southern Tibet: Response to slab dynamics and erosion. *Geology, 42*(5), 443-446. https://doi.org/10.1130/G35350.1

Clift, P., Schlup, M., Carter, A., & Steck, A. (2004). Discussion of exhumation history of eastern Ladakh revealed by 40Ar/39Ar and fission track ages: the Indus River–Tso Morari transect, NW Himalaya. *Journal of the Geological Society, 161*(5), 893-894. https://doi.org/10.1144/0016-764903-104

Clift, P. D., Carter, A., Krol, M., & Kirby, E. (2002). Constraints on India-Eurasia collision in the Arabian Sea region taken from the Indus Group, Ladakh Himalaya, India. In P. D. Clift, D. Kroon, C. Gaedicke, & J. Craig (Eds.), *The Tectonic and Climatic Evolution of the Arabian Sea Region: Geological Society, London, Special Publication 195* (pp. 97-116). https://doi.org/10.1144/gsl.Sp.2002.195.01.07

Coutts, D. S., Matthews, W. A., & Hubbard, S. M. (2019). Assessment of widely used methods to derive depositional ages from detrital zircon populations. *Geoscience Frontiers, 10*(4), 1421-1435. https://doi.org/10.1016/j.gsf.2018.11.002

DeCelles, P. G., Kapp, P., Quade, J., & Gehrels, G. E. (2011). Oligocene-Miocene Kailas basin, southwestern Tibet: Record of postcollisional upper-plate extension in the Indus-Yarlung suture zone. *Geological Society of America Bulletin, 123*(7-8), 1337-1362. https://doi.org/10.1130/b30258.1

Dickinson, W. R., & Gehrels, G. E. (2009). Use of U–Pb ages of detrital zircons to infer maximum depositional ages of strata: A test against a Colorado Plateau Mesozoic database. *Earth and Planetary Science Letters, 288*(1-2), 115-125. https://doi.org/10.1016/j.epsl.2009.09.013

Dumitru, T. A. (1991). Effects of subduction parameters on geothermal gradients in forearcs, with an application to Franciscan Subduction in California. *Journal of Geophysical Research: Solid Earth, 96*(B1), 621-641. https://doi.org/10.1029/90jb01913

Ehlers, T. A., & Farley, K. A. (2003). Apatite (U–Th)/He thermochronometry: methods and applications to problems in tectonic and surface processes. *Earth and Planetary Science Letters, 206*(1-2), 1-14. https://doi.org/10.1016/S0012-821X(02)01069-5

Epard, J.-L., & Steck, A. (2008). Structural development of the Tso Morari ultra-high pressure nappe of the Ladakh Himalaya. *Tectonophysics, 451*(1-4), 242-264. https://doi.org/10.1016/j.tecto.2007.11.050

Farley, K., Wolf, R., & Silver, L. (1996). The effects of long alpha-stopping distances on (U Th)/He ages. *Geochimica et cosmochimica acta, 60*(21), 4223-4229. https://doi.org/10.1016/S0016-7037(96)00193-7

Garzanti, E., Baud, A., & Mascle, G. (1987). Sedimentary record of the northward flight of India and its collision with Eurasia (Ladakh Himalaya, India). *Geodinamica Acta, 1*(4/5), 297-312. https://doi.org/10.1080/09853111.1987.11105147

Garzanti, E., & Van Haver, T. (1988). The Indus clastics: forearc basin sedimentation in the Ladakh Himalaya (India). *Sedimentary Geology, 59*(3-4), 237-249. https://doi.org/10.1016/0037-0738(88)90078-4

Ge, Y.-K., Dai, J.-G., Wang, C.-S., Li, Y.-L., Xu, G.-Q., & Danisik, M. (2017). Cenozoic thermo-tectonic evolution of the Gangdese batholith constrained by low-temperature thermochronology. *Gondwana Research, 41*, 451-462. https://doi.org/10.1016/j.gr.2016.05.006

Green, O. R., Searle, M. P., Corfield, R. I., & Corfield, R. M. (2008). Cretaceous-Tertiary Carbonate Platform Evolution and the Age of the India-Asia Collision along the Ladakh Himalaya (Northwest India). *The Journal of Geology, 116*(4), 331-353. https://doi.org/10.1086/588831

Guenthner, W. R., Reiners, P. W., Ketcham, R. A., Nasdala, L., & Giester, G. (2013). Helium diffusion in natural zircon: Radiation damage, anisotropy, and the interpretation of zircon (U-Th)/He thermochronology. *American Journal of Science, 313*(3), 145-198. https://doi.org/10.2475/03.2013.01

Henderson, A. L., Najman, Y., Parrish, R., BouDagher-Fadel, M., Barford, D., Garzanti, E., & Andò, S. (2010). Geology of the Cenozoic Indus Basin sedimentary rocks: Paleoenvironmental interpretation of sedimentation from the western Himalaya during the early phases of India-Eurasia collision. *Tectonics, 29*(6), n/a-n/a. https://doi.org/10.1029/2009tc002651

Henderson, A. L., Najman, Y., Parrish, R., Mark, D. F., & Foster, G. L. (2011). Constraints to the timing of India–Eurasia collision; a re-evaluation of evidence from the Indus Basin sedimentary rocks of the Indus–Tsangpo Suture Zone, Ladakh, India. *Earth-Science Reviews, 106*(3-4), 265-292. https://doi.org/10.1016/j.earscirev.2011.02.006

Hurford, A. J. (1986). Cooling and uplift patterns in the Lepontine Alps South Central Switzerland and an age of vertical movement on the Insubric fault line. *Contributions to Mineralogy and Petrology, 92*(4), 413-427. https://doi.org/10.1007/BF00374424

Hurford, A. J. (1990). Standardization of fission track dating calibration: Recommendation by the Fission Track Working Group of the I.U.G.S. Subcommission on Geochronology. *Chemical Geology: Isotope Geoscience section, 80*(2), 171-178. https://doi.org/10.1016/0168-9622(90)90025-8

Hurford, A. J., & Green, P. F. (1983). The zeta age calibration of fission-track dating. *Chemical Geology, 41*, 285-317. https://doi.org/10.1016/S0009-2541(83)80026-6

Kapp, P., & DeCelles, P. G. (2019). Mesozoic–Cenozoic geological evolution of the Himalayan-Tibetan orogen and working tectonic hypotheses. *American Journal of Science, 319*(3), 159-254. https://doi.org/10.2475/03.2019.01

Ketcham, R. A. (2005). Forward and Inverse Modeling of Low-Temperature Thermochronometry Data. Reviews in Mineralogy and Geochemistry, 58(1), 275-314. doi: https://doi.org/10.2138/rmg.2005.58.11

Kirstein, L. A., Foeken, J. P. T., van der Beek, P., Stuart, F. M., & Phillips, R. J. (2009). Cenozoic unroofing history of the Ladakh Batholith, western Himalaya, constrained by thermochronology and numerical modelling. *Journal of the Geological Society, 166*(4), 667-678. https://doi.org/10.1144/0016-76492008-107

Kirstein, L. A., Sinclair, H., Stuart, F. M., & Dobson, K. (2006). Rapid early Miocene exhumation of the Ladakh batholith, western Himalaya. *Geology, 34*(12). https://doi.org/10.1130/g22857a.1

Kumar, R., Jain, A., Lal, N., & Singh, S. (2017). Early–Middle Eocene exhumation of the Trans-Himalayan Ladakh Batholith, and the India–Asia convergence. *CURRENT SCIENCE, 113*(6), 1090.

679 Langille, J. M., Jessup, M. J., Cottle, J., & Ahmad, T. (2014). Kinematic and thermal studies of
680 the Leo Pargil Dome: Implications for synconvergent extension in the NW Indian
681 Himalaya. *Tectonics, 33*(9), 1766-1786. https://doi.org/10.1002/2014tc003593

682 Laskowski, A. K., Kapp, P., & Cai, F. (2018). Gangdese culmination model: Oligocene–Miocene
683 duplexing along the India-Asia suture zone, Lazi region, southern Tibet. *GSA Bulletin,*
684 *130*(7-8), 1355-1376. https://doi.org/10.1130/b31834.1

685 Li, G., Kohn, B., Sandiford, M., & Xu, Z. (2017). India-Asia convergence: Insights from burial
686 and exhumation of the Xigaze fore-arc basin, south Tibet. *Journal of Geophysical*
687 *Research: Solid Earth, 122*(5), 3430-3449. https://doi.org/10.1002/2017jb014080

688 Li, G., Kohn, B., Sandiford, M., Xu, Z., Tian, Y., & Seiler, C. (2016). Synorogenic
689 morphotectonic evolution of the Gangdese batholith, South Tibet: Insights from low-
690 temperature thermochronology. *Geochemistry, Geophysics, Geosystems, 17*(1), 101-112.
691 https://doi.org/10.1002/2015gc006047

692 Li, G., Tian, Y., Kohn, B. P., Sandiford, M., Xu, Z., & Cai, Z. (2015). Cenozoic low temperature
693 cooling history of the Northern Tethyan Himalaya in Zedang, SE Tibet and its
694 implications. *Tectonophysics, 643*, 80-93. https://doi.org/10.1016/j.tecto.2014.12.014

695 Mathur, N. (1983). The Indus Formation of the Ladakh Himalaya: its biozonation, correlation
696 and faunal provincialism. In (eds) Thakur, V.C. & Sharma, K.K. (Eds.), *Geology of Indus*
697 *Suture Zone of Ladakh*: *Professor DN Wadia Birth Centenary Commemorative Volume.*
698 *Wadia Institute of Himalayan Geology*, (pp. 127-144).

699 Najman, Y. (2006). The detrital record of orogenesis: A review of approaches and techniques
700 used in the Himalayan sedimentary basins. *Earth-Science Reviews*.
701 https://doi.org/10.1016/j.earscirev.2005.04.004

702 Ning, Z., Zhang, L., Huntington, K. W., Wang, C., Dai, J., Han, Z., . . . Zhang, J. (2019). The
703 burial and exhumation history of the Liuqu Conglomerate in the Yarlung Zangbo suture
704 zone, southern Tibet: Insights from clumped isotope thermometry. *Journal of Asian*
705 *Earth Sciences, 174*, 205-217. https://doi.org/10.1016/j.jseaes.2018.12.009

706 Orme, D. A. (2019). Burial and exhumation history of the Xigaze forearc basin, Yarlung suture
707 zone, Tibet. *Geoscience Frontiers, 10*(3), 895-908.
708 https://doi.org/10.1016/j.gsf.2017.11.011

709 Reiners, P. W. (2005). Zircon (U-Th)/He Thermochronometry. Reviews in Mineralogy and
710 Geochemistry, 58(1), 151-179. doi: https://doi.org/10.2138/rmg.2005.58.6

711 Robertson, A., & Sharp, I. (1998). Mesozoic deep-water slope/rise sedimentation and volcanism
712 along the North-Indian passive margin: evidence from the Karamba Complex, Indus
713 suture zone (Western Ladakh Himalaya). *Journal of Asian Earth Sciences, 16*(2-3), 195-
714 215. https://doi.org/10.1016/S0743-9547(98)00010-5

715 Schlup, M., Carter, A., Cosca, M., & Steck, A. (2003). Exhumation history of eastern Ladakh

revealed by 40Ar/39Ar and fission-track ages: the Indus River–Tso Morari transect, NW Himalaya. *Journal of the Geological Society, 160*(3), 385-399. https://doi.org/10.1144/0016-764902-084

Schlup, M., Steck, A., Carter, A., Cosca, M., Epard, J.-L., & Hunziker, J. (2011). Exhumation history of the NW Indian Himalaya revealed by fission track and 40Ar/39Ar ages. *Journal of Asian Earth Sciences, 40*(1), 334-350. https://doi.org/10.1016/j.jseaes.2010.06.008

Searle, M., Corfield, R. I., Stephenson, B., & McCarron, J. (1997). Structure of the North Indian continental margin in the Ladakh–Zanskar Himalayas: implications for the timing of obduction of the Spontang ophiolite, India–Asia collision and deformation events in the Himalaya. *Geological Magazine, 134*(3), 297-316. https://doi.org/10.1017/S0016756897006857

Searle, M. P. (1996). Geological evidence against large-scale pre-Holocene offsets along the Karakoram Fault: Implications for the limited extrusion of the Tibetan plateau. *Tectonics, 15*(1), 171-186. https://doi.org/10.1029/95tc01693

Searle, M. P. (2019). Timing of subduction initiation, arc formation, ophiolite obduction and India–Asia collision in the Himalaya. In P. J. Treloar & M. P. Searle (Eds.), *Himalayan Tectonics: A Modern Synthesis: Geological Society, London, Special Publication 483* (pp. 19-37). https://doi.org/10.1144/sp483.8

Searle, M. P., Pickering, K. T., & Cooper, D. J. W. (1990). Restoration and evolution of the intermontane lndus molasse basin, Ladakh Himalaya, India. *Tectonophysics, 174*(3-4), 301-314. https://doi.org/10.1016/0040-1951(90)90327-5

Searle, M. P., Waters, D. J., Rex, D. C., & Wilson, R. N. (1992). Pressure, temperature and time constraints on Himalayan metamorphism from eastern Kashmir and western Zanskar. *Journal of the Geological Society, 149*(5), 753-773. https://doi.org/10.1144/gsjgs.149.5.0753

Sinclair, H. D., & Jaffey, N. (2001). Sedimentology of the Indus Group, Ladakh, northern India: implications for the timing of initiation of the palaeo-Indus River. *Journal of the Geological Society [London], 158*(1), 151-162. https://doi.org/10.1144/jgs.158.1.151

Singh, I. B., Sahni, A., Jain, A. K., Upadhyay, R., Parcha, S. K., Parmar, V., . . . Ahmad, S. (2015). Post-collision sedimentation in the Indus Basin (Ladakh, India): Implications for the evolution of the northern margin of the Indian Plate. *Journal of the Palaeontological Society of India, 60*(2), 97-146.

Steck, A. (2003). Geology of the NW Indian Himalaya. Ecologae Geologicae Helvetiae, *96*, 147-196. https://doi.org/10.1007/s00015-003-1091-4

St-Onge, M. R., Rayner, N., & Searle, M. P. (2010). Zircon age determinations for the Ladakh batholith at Chumathang (Northwest India): Implications for the age of the India–Asia collision in the Ladakh Himalaya. Tectonophysics, 495(3-4), 171-183. doi:

https://doi.org/10.1016/j.tecto.2010.09.010

Tremblay, M. M., Fox, M., Schmidt, J. L., Tripathy-Lang, A., Wielicki, M. M., Harrison, T. M., . . . Shuster, D. L. (2015). Erosion in southern Tibet shut down at approximately 10 Ma due to enhanced rock uplift within the Himalaya. *Proceedings of the National Academy of Sciences USA, 112*(39), 12030-12035. https://doi.org/10.1073/pnas.1515652112

Tripathy-Lang, A., Hodges, K. V., van Soest, M. C., & Ahmad, T. (2013). Evidence of pre-Oligocene emergence of the Indian passive margin and the timing of collision initiation between India and Eurasia. *Lithosphere, 5*(5), 501-506. https://doi.org/10.1130/l273.1

Van Haver, T. (1984). *Etude stratigraphique, sédimentologique et structurale d'un bassin d'avant arc: exemple du bassin de l'Indus, Ladakh, Himalaya*. Université Scientifique et Médicale de Grenoble. https://tel.archives-ouvertes.fr/tel-00641418v2

Van Haver, T., Bonhomme M. G., Mascle G., and Aprahamian J. (1986), Analyses K/Ar de phyllites fines des formations détritiques de l'Indus au Ladakh (Inde): Mise en evidence de l'âge éocène supérieur du métamorphisme. *Comptes rendus de l'Académie des sciences., Serie 2*, *302*(6), 325-330.

Vermeesch, P. (2009). RadialPlotter: A Java application for fission track, luminescence and other radial plots. *Radiation Measurements, 44*(4), 409-410. https://doi.org/10.1016/j.radmeas.2009.05.003

Walsh, J. M. J., Buckman, S., Nutman, A. P., & Zhou, R. (2019). Age and Provenance of the Nindam Formation, Ladakh, NW Himalaya: Evolution of the Intraoceanic Dras Arc Before Collision With India. *Tectonics, 38*(8), 3070-3096. https://doi.org/10.1029/2019tc005494

Webb, A. A. G., Guo, H., Clift, P. D., Husson, L., Müller, T., Costantino, D., . . . Wang, Q. (2017). The Himalaya in 3D: Slab dynamics controlled mountain building and monsoon intensification. *Lithosphere*. https://doi.org/10.1130/l636.1

Weinberg, R. F., & Dunlap, W. J. (2000). Growth and Deformation of the Ladakh Batholith, Northwest Himalayas: Implications for Timing of Continental Collision and Origin of Calc-Alkaline Batholiths. *Journal of Geology, 108*(3), 303-320. https://doi.org/10.1086/314405

Wu, F.-Y., Clift, P. D., & Yang, J.-H. (2007). Zircon Hf isotopic constraints on the sources of the Indus Molasse, Ladakh Himalaya, India. *Tectonics, 26*(2), TC2014 https://doi.org/10.1029/2006tc002051

Zeitler, P. K. (1985). Cooling history of the NW Himalaya, Pakistan. Tectonics, 4(1), 127-151. doi: https://doi.org/10.1029/TC004i001p00127

Zhang, R., Murphy, M. A., Lapen, T. J., Sanchez, V., & Heizler, M. (2011). Late Eocene crustal thickening followed by Early-Late Oligocene extension along the India-Asia suture zone: Evidence for cyclicity in the Himalayan orogen. *Geosphere, 7*(5), 1249-1268.

https://doi.org/10.1130/GES00643.1

Zhu, C., Rao, S., & Hu, S. (2016). Application of illite crystallinity for paleo-temperature reconstruction: A case study in the western Sichuan basin, SW China. *Carpathian Journal of Earth and Environmental Sciences, 11*(2), 599-608.

Zhuang, G., Najman, Y., Guillot, S., Roddaz, M., Antoine, P.-O., Métais, G., . . . Solangi, S. H. (2015). Constraints on the collision and the pre-collision tectonic configuration between India and Asia from detrital geochronology, thermochronology, and geochemistry studies in the lower Indus basin, Pakistan. *Earth and Planetary Science Letters, 432*, 363-373. https://doi.org/10.1016/j.epsl.2015.10.026

Figure Captions

Figure 1. Geological map of the India-Asia collision zone in Ladakh, NW India showing major tectono-stratigraphic units modified after Buchs and Epard (2019). Studied cross-sections are indicated in red: 1 - Temesgam section; 2 - Basgo section; 3 - Zanskar Gorge; 4 - Upshi-Lato section. Bottom Left: Location of the study area (red) with respect to major terranes of south Asia. Blackened zones contain ophiolites. Bottom Right: Schematic cross-section along AA' through the collision zone in NW India.

Figure 2. Geological maps of **(A)** Temesgam (1) and Basgo (2) sections (numbered in red; modified after Garzanti and Van Haver, 1988; Tripathy-Lang et al., 2013), **(B)** Zanskar Gorge (modified after Henderson et al. 2010), and **(C)** Upshi-Lato section (modified after Henderson et al. 2011) showing formations, major structures and our sample locations. Abbreviations: Fm - Formation, sh - shale, Conglomerate - cgl, N lst - Nummulitic Limestone, U - upper, M - middle, L - lower, R - river.

Figure 3. A. Plot showing range of ZFT ages from the Zanskar Gorge samples. Vertical black lines specify ZFT age ranges for each sample and contain solid black diamonds that indicate corresponding depositional ages. Mean percentage of grains representing modes M1, M2, M3 and M4, determined from Abanico plots, are shown in parantheses. Abbreviations: Congl. - Conglomerate; Numm. Lst. - Nummulitic Limestone; n - number of grains. Solid black diamonds indicate depositional ages. **B.** Zircon (ZHe) and apatite (AHe) (U-Th)/He ages versus stratigraphic ages of the Indus Basin sedimentary rocks (IBSR). The ZHe ages (2-3 grains per sample) of individual grains are indicated by the horizontal bars on the dark grey rectangles. The AHe ages (5 grains per sample) are represented by light grey box and whisker plots, where the whiskers represent maximum and minimum individual apatite ages. Solid black squares indicate depositional ages. * - The depositonal age of the Lato Formation is Late Cretaceous, which is not shown on the vertical scale. The depositional ages are compiled from Bajpai et al. (2004), Wu et al., (2007), Henderson et al. (2010, 2011) and Bhattacharya (2020).

Figure 4. Time-temperature *(t-T)* models of the IBSR extracted from HeFTy program (Ketcham, 2005). **(A)** Lato Formation, **(B)** Sumdo Formation, **(C)** Lower Upshi Formation, **(D)** Basgo Formation, and **(E)** Temesgam Formation. Abbreviations: PT - paths tried, AP (green) -acceptable paths, GP (pink) -good paths. Solid black line indicates best fit model path. Hollow square boxes demarcate *t-T* constraints.

827 **Table Captions**

828 **Table 1.** Published stratigraphic schemes compared across the IBSR sections in NW India.

829 **Table 2.** Summary of ZFT, ZHe and AHe ages from Zanskar Gorge, Upshi-Lato, Basgo and Temesgam
830 sections.

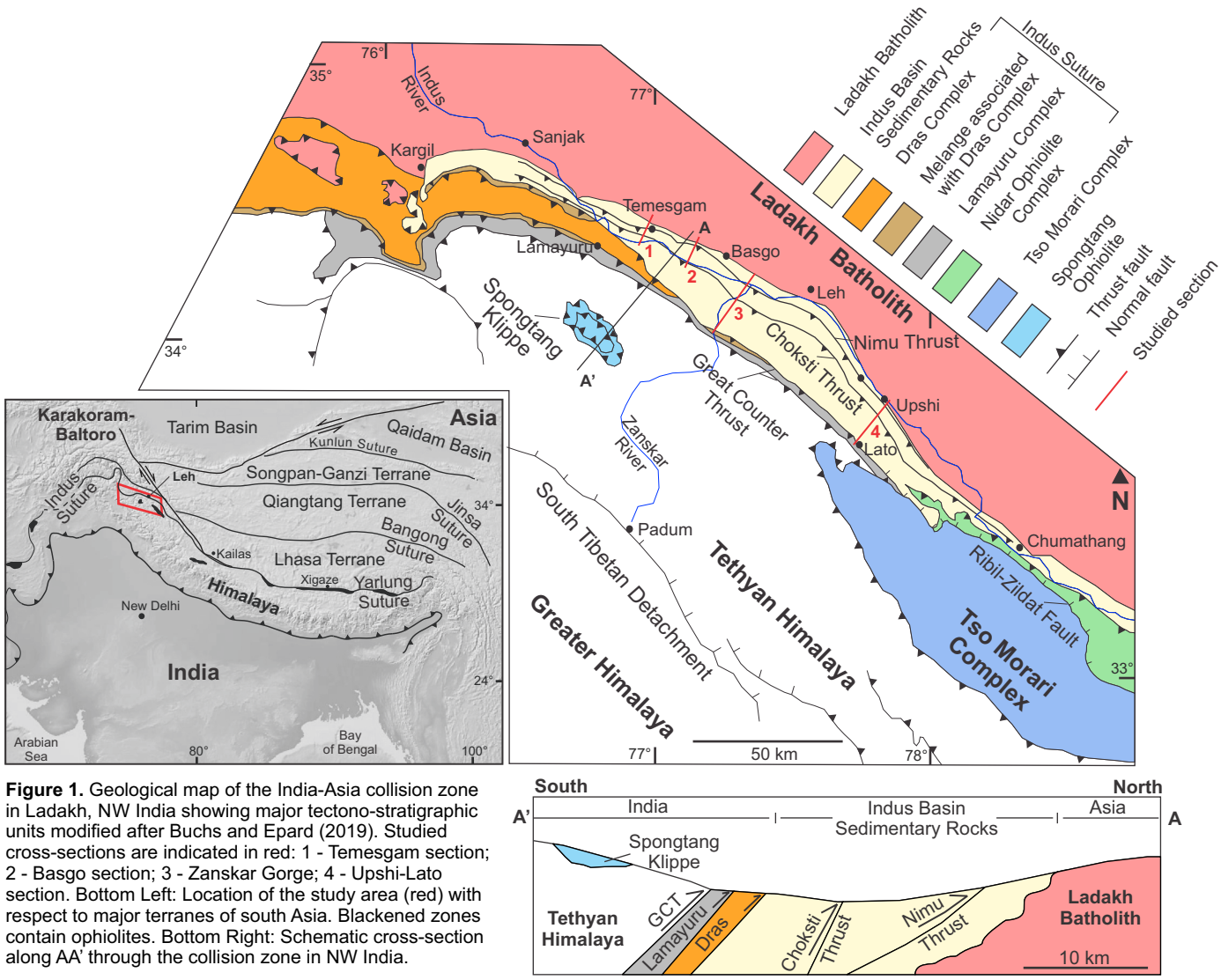

Figure 1. Geological map of the India-Asia collision zone in Ladakh, NW India showing major tectono-stratigraphic units modified after Buchs and Epard (2019). Studied cross-sections are indicated in red: 1 - Temesgam section; 2 - Basgo section; 3 - Zanskar Gorge; 4 - Upshi-Lato section. Bottom Left: Location of the study area (red) with respect to major terranes of south Asia. Blackened zones contain ophiolites. Bottom Right: Schematic cross-section along AA' through the collision zone in NW India.

Bhattacharya et al. (Figure 1)

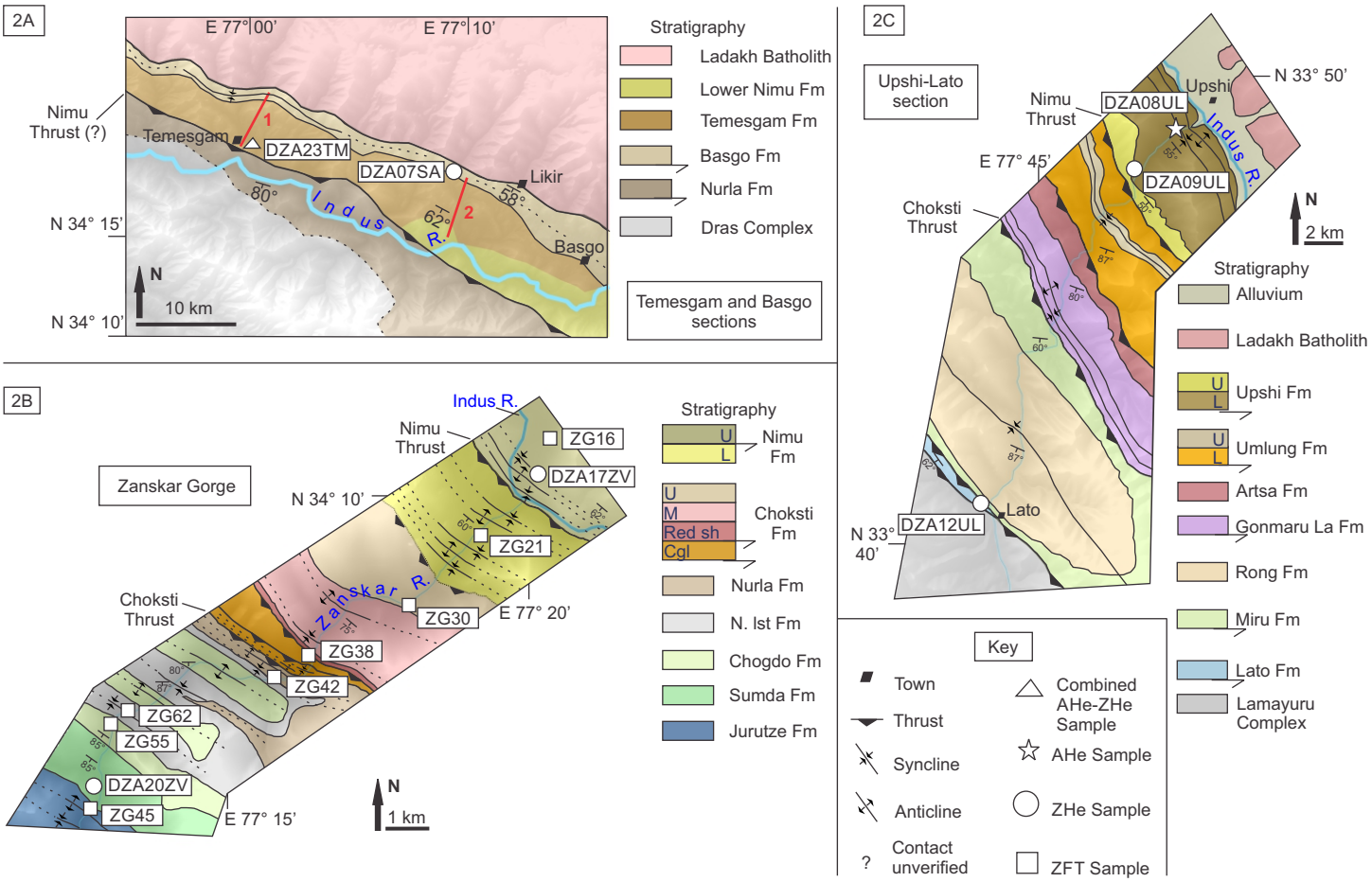

Figure 2. Geological maps of (A) Temesgam (1) and Basgo (2) sections (numbered in red; modified after Garzanti and Van Haver, 1988; Tripathy-Lang et al., 2013), (B) Zanskar Gorge (modified after Henderson et al. 2010), and (C) Upshi-Lato section (modified after Henderson et al. 2011) showing formations, major structures and our sample locations. Abbreviations: Fm - Formation, sh - shale, Conglomerate - cgl, N lst - Nummulitic Limestone, U - upper, M - middle, L - lower, R - river.

Bhattacharya et al. (Figure 2)

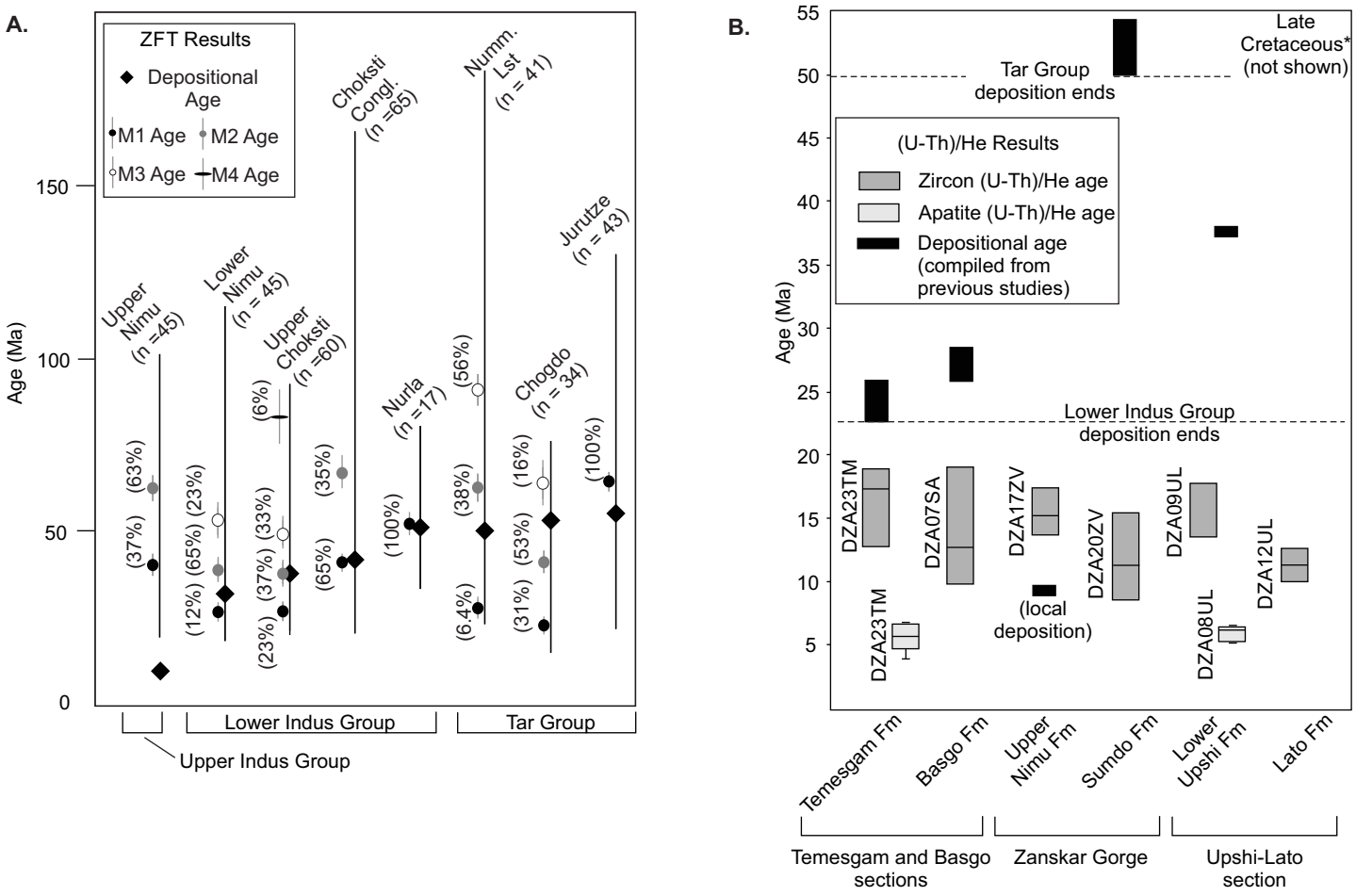

Figure 3. A. Plot showing range of ZFT ages from the Zanskar Gorge samples. Vertical black lines specify ZFT age ranges for each sample and contain solid black diamonds that indicate corresponding depositional ages. Mean percentage of grains representing modes M1, M2, M3 and M4, determined from Abanico plots, are shown in parantheses. Abbreviations: Congl. - Conglomerate; Numm. Lst. - Nummulitic Limestone; n - number of grains.
B. Zircon (ZHe) and apatite (AHe) (U-Th)/He ages versus stratigraphic ages of the Indus Basin sedimentary rocks (IBSR). The ZHe ages (2-3 grains per sample) of individual grains are indicated by the horizontal bars on the dark grey rectangles. The AHe ages (5 grains per sample) are represented by light grey box and whisker plots, where the whiskers represent maximum and minimum individual apatite ages. Solid black squares indicate depositional ages. * - The depositonal age of the Lato Formation is Late Cretaceous, which is not shown on the vertical scale. The depositional ages are compiled from Bajpai et al. (2004), Wu et al., (2007), Henderson et al. (2010, 2011) and Bhattacharya (2020).

Bhattacharya et al. (Figure 3)

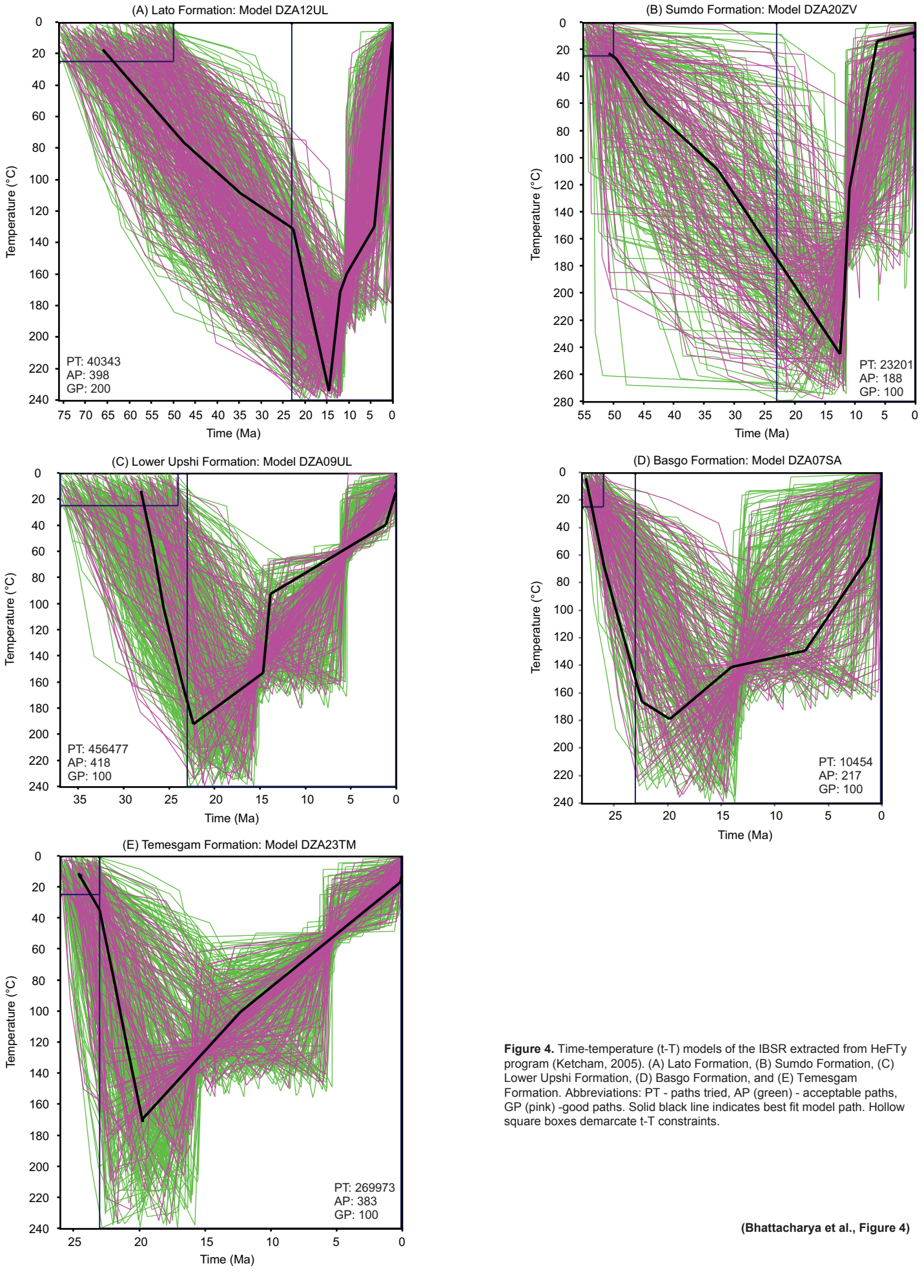

Figure 4. Time-temperature (t-T) models of the IBSR extracted from HeFTy program (Ketcham, 2005). (A) Lato Formation, (B) Sumdo Formation, (C) Lower Upshi Formation, (D) Basgo Formation, and (E) Temesgam Formation. Abbreviations: PT - paths tried, AP (green) - acceptable paths, GP (pink) -good paths. Solid black line indicates best fit model path. Hollow square boxes demarcate t-T constraints.

(Bhattacharya et al., Figure 4)